RSC Advances

PAPER

View Article Online
View Journal | View Issue

Cite this: *RSC Adv.*, 2017, **7**, 11123

Nanorod-assembled $NiCo_2O_4$ hollow microspheres assisted by an ionic liquid as advanced electrode materials for supercapacitors†

Yirong Zhu,[ab] Xiaobo Ji,[c] Ruiming Yin,[b] Zhongliang Hu,[b] Xiaoqing Qiu,[c] Zhibin Wu[c] and Yong Liu*[a]

Received 3rd January 2017
Accepted 24th January 2017

DOI: 10.1039/c7ra00067g

rsc.li/rsc-advances

In this work, nanorod-assembled $NiCo_2O_4$ hollow microspheres have been successfully prepared by an ionic liquid-assisted hydrothermal method for the first time. The as-obtained nanorod-assembled $NiCo_2O_4$ hollow microspheres manifest a high specific capacitance (764 F g^{-1} at 2 A g^{-1}), exceptional rate capability (53.5% of capacity retention at 30 A g^{-1}) and good cycling stability (101.7% of initial capacity retention after 1500 cycles). The superior electrochemical performance can be attributed to the unique hollow micro-/nanostructure, which can provide more active sites for the faradic redox reaction, provide an easy electrolyte penetration path and alleviate the volume change during the charge–discharge process. These results suggest that the nanorod-assembled $NiCo_2O_4$ hollow microspheres could be promising electrode materials for supercapacitor applications. Additionally, this synthetic method can be extended to the fabrication of other hollow micro-/nanostructure materials for energy and other related applications.

1. Introduction

With the increasing depletion of traditional fossil fuels and the worsening of environmental pollution, new renewable energy storage technologies have been attracting more and more research interest.[1–3] As a new energy storage device, the supercapacitor has recently attracted tremendous attention and research due to its advantages such as high power density, fast charge/discharge rate capability, and long cycle span.[4,5] Currently, the research of supercapacitors is mainly focused on the electrode material, electrolyte and assembly technology. The properties of supercapacitors are mainly determined by the electrode material, thus the study of electrode materials has become a research hotspot. Among these electrode materials, ternary metal oxides ($NiCo_2O_4$) are emerging as a promising electrode material for supercapacitors.[6,7] The coupling of nickel and cobalt ions render the $NiCo_2O_4$ with richer redox reactions and better electronic conductivity than single-component NiO and Co_3O_4, which are beneficial to the improvement of the electrochemical performances. Moreover, $NiCo_2O_4$ has several inherent advantages of low cost, natural abundance and low toxicity. These attractive features make $NiCo_2O_4$ a promising cost-effective and superior electrode material for supercapacitors.

Recently, the study of $NiCo_2O_4$ has been focused on the synthesis of various special morphologies, including nanowires,[8,9] nanoneedles,[10] nanorods,[11] nanotubes,[12] nanosheets,[13,14] 3D structures,[15,16] urchin-like structures,[17] and hollow structures.[18–20] Among these morphologies, hollow micro-/nanostructures have drawn extensive attention because of their attractive advantages such as a large specific surface area, low density, a kinetically favorable open structure and surface permeability, which can achieve an enhancement of the electrochemical performances.[21,22] Yuan *et al.*[18] reported the use of silica spheres as a hard template to synthesize hollow $NiCo_2O_4$ sub-microspheres delivering superior electrochemical properties as supercapacitor electrode materials. Lou *et al.*[19] developed a self-templated strategy to prepare uniform $NiCo_2O_4$ hollow spheres with complex interior structures showing superior electrochemical performances as advanced electrode materials for both lithium-ion batteries and supercapacitors. Very recently, our group has fabricated mesoporous $NiCo_2O_4$ hollow microspheres utilizing a soft template method *via* a hydrothermal synthesis route, demonstrating enhanced specific capacitance, rate capability and cycling stability compared to solid microspheres and collapsed hollow microspheres.[20] However, to the best of our knowledge, there is still

[a]*State Key Lab of Powder Metallurgy, Central South University, Changsha, 410083, China. E-mail: yonliu@csu.edu.cn; Fax: +86-731-88710855; Tel: +86-731-88876630*
[b]*College of Metallurgy and Material Engineering, Hunan University of Technology, Zhuzhou, 412007, China. E-mail: zhuyirong2004@163.com; Fax: +86-731-22183470; Tel: +86-731-22183470*
[c]*College of Chemistry and Chemical Engineering, Central South University, Changsha, 410083, China. E-mail: xji@csu.edu.cn; Fax: +86-731-88879616; Tel: +86-731-88879616*

† Electronic supplementary information (ESI) available: Nitrogen adsorption and desorption isotherm and the corresponding BJH pore size distribution curve of the $NiCo_2O_4$ hollow microspheres. See DOI: 10.1039/c7ra00067g

no report on the fabrication of nanorod-assembled $NiCo_2O_4$ hollow microspheres using an ionic liquid-assisted hydrothermal synthesis route.

Ionic liquids, which are typically composed of hydrophilic inorganic anions and hydrophobic organic cations, are a kind of environmentally friendly green solvent.[23,24] They have many superior advantages compared with common organic solvents and surfactants, and they have been used as templates and solvents in the synthesis of inorganic materials with unique morphologies, resulting in improved electrochemical properties.[25–28] However, reports of ionic liquid-assisted syntheses of inorganic materials are still rare, especially for applications in the field of supercapacitors. Recently, Xu *et al.*[29] successfully fabricated C_3N_4/a-Fe_2O_3 hollow microspheres with enhanced supercapacitive performance utilizing an ionic liquid-assisted solvothermal method. The study reveals that the used ionic liquid 1-butyl-3-methylimidazolium tetrachlorideferrate(III) [Bmim]$FeCl_4$ acts as solvent, template and reactant during the synthesis process, and plays a vital role in the formation of hollow microspheres. Thus, utilizing ionic liquids to synthesize superior supercapacitor electrode materials is an attractive prospect.

Herein, a facile ionic liquid [Bmim]Cl-assisted hydrothermal method was utilized to prepare nanorod-assembled $NiCo_2O_4$ hollow microspheres for the first time. During the synthesis process, the ionic liquid acts not only as the solvent but also as the template, and a possible formation mechanism of the $NiCo_2O_4$ hollow microspheres is proposed. The as-resulted $NiCo_2O_4$ hollow microspheres were used as electrode materials for supercapacitors and superior electrochemical properties could be obtained.

2. Experiment section

2.1 Materials and chemicals

All the chemicals purchased in the experiments were used without further purification. $NiCl_2 \cdot 6H_2O$ (analytical grade) and $CoCl_2 \cdot 6H_2O$ (analytical grade) were obtained from Fengchuan Chemical Reagent Co., Ltd, Tianjin. $CO(NH_2)_2$ (analytical grade) was bought from Xilong Chemical Co., Ltd. [Bmim]Cl (analytical grade) was purchased from Sinopharm Chemical Reagent Beijing Co., Ltd.

2.2 Materials synthesis

In a typical synthesis, 2 mmol of $NiCl_2 \cdot 6H_2O$ and 4 mmol of $CoCl_2 \cdot 6H_2O$ were dissolved in 20 mL of distilled water. Then, 10 g of the ionic liquid [Bmim]Cl was added into the mixed solution under stirring. Subsequently, 30 mmol of $CO(NH_2)_2$ was further added into the above mixed solution. After stirring for 30 min, the solution was transferred to a Teflon-lined stainless steel autoclave and heated in an oven at 120 °C for 10 h. After being cooled to room temperature, the precipitate was collected by centrifugation, washed with deionized water and absolute ethanol several times, and finally dried in a vacuum oven at 60 °C for 12 h. Finally, the precursor was further annealed at 300 °C in air for 3 h to obtain the product.

2.3 Materials characterization

Thermogravimetric (TG) data of the sample was acquired using a thermal analysis instrument (NETZSCH STA449F3) from room temperature to 800 °C in air. The X-ray diffraction (XRD) pattern of the sample was collected using a Rigaku D/max 2550 VB^+ 18 kW X-ray diffractometer with Cu Kα radiation at a scanning rate of 0.1° 2θ s^{-1}. The morphology of the sample was examined using scanning electron microscopy (SEM, JSM-6510LV). The Brunauer–Emmett–Teller (BET, BELSORP-MINIII) specific surface area and the pore size distribution wereacquired based on the N_2 adsorption/desorption measurement.

2.4 Electrochemical characterization

The working electrode was prepared by mixing 70 wt% of $NiCo_2O_4$, 20 wt% of carbon black (super P), and 10 wt% of polyvinylidene difluoride (PVDF) with a few drops of *N*-methyl-2-pyrrolidine (NMP). The mixture was then coated onto nickel foam as a current collector, which was pretreated according to our previous work.[16,20,30,31] The prepared electrode was dried under a vacuum at 100 °C for 10 h and then pressed under a pressure of 15 MPa for 30 s. The electrolyte used was 2 M KOH aqueous solution. The electrochemical properties of the sample were evaluated using a CHI 660D electrochemical workstation using cyclic voltammetry (CV) and galvanostatic charge–discharge tests with a three-electrode system where Pt foil served as the counter electrode and Hg/HgO as the reference electrode.

3. Results and discussion

Thermogravimetric analysis (TG) was employed to determine the optimum calcination temperature of the as-prepared sample. The TGA curve of the $NiCo_2O_4$ precursor is shown in Fig. 1. The initial weight loss between room temperature and 220 °C is due to the removal of physically adsorbed water and crystal water. The second obvious weight loss between 220 and 300 °C corresponds to the conversion of the precursor to $NiCo_2O_4$. Beyond 300 °C, no obvious weight loss can be observed, demonstrating the formation of the stable $NiCo_2O_4$

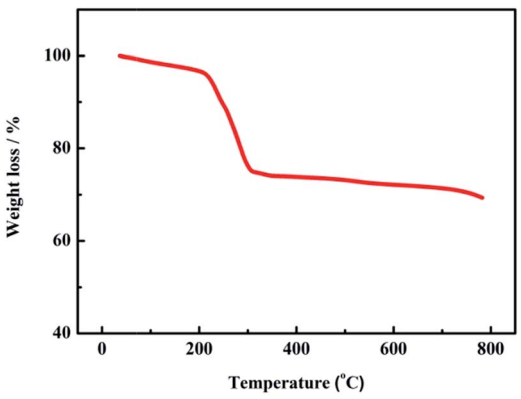

Fig. 1 TG curve of the nanorod-assembled $NiCo_2O_4$ hollow microspheres precursor.

product. Based on the thermal analysis, 300 °C is chosen as the calcination temperature in this work.

The phase and composition of the as-prepared sample were analyzed using X-ray diffraction (XRD), as shown in Fig. 2. The positions and intensities of the characteristic peaks agree well with the standard pattern of the cubic spinel $NiCo_2O_4$ phase (JCPDS card no. 20-0781). The characteristic peaks at 18.91°, 31.15°, 36.70°, 38.40°, 44.62°, 55.44°, 59.09°, 64.98° and 68.31° are indexed to the (111), (220), (311), (222), (400), (422), (511), (440) and (531) planes of cubic spinel $NiCo_2O_4$, respectively.

In order to investigate the morphology of the as-prepared sample, SEM was performed, as displayed in Fig. 3. It can be observed from Fig. 3a and b that the morphology of the sample is an urchin-like structure with an average diameter of 3–5 μm. As shown in Fig. 3c, the image of the broken microsphere indicates the hollow structure, and the shell of the hollow microsphere is composed of an aggregation of many tiny nanorods. In addition, it can be seen from Fig. 3d that a large quantity of open holes exist between the interconnected nanorods. Such a unique hollow micro/nanostructure indicates a relatively high specific surface area and abundant porosity structure, which is further confirmed by the BET N_2 adsorption/desorption measurements in Fig. S1.† The BET characterization reveals that the specific surface area is 38.9 $m^2 g^{-1}$, and the pore size distribution is mainly centered in the mesoporous size range of 10–30 nm with an average pore diameter of 19.4 nm. Although the specific surface area of the as-obtained $NiCo_2O_4$ hollow microspheres is not high enough, the mesoporous structure with a relatively large pore size and the outstanding electronic conductivity reported by many previous studies[32,33] are particularly favorable for the fast diffusion of electrolyte ions and the transport of electrons during the charge–discharge process, resulting in the enhancement of the electrochemical performance. It is well-known that the specific surface area and electronic conductivity usually have an opposite effect on the supercapacitive performance.[34] Thus, in order to obtain superior electrochemical performance, it is vitally important to balance the specific surface area, pore structure and electronic conductivity in the preparation process.

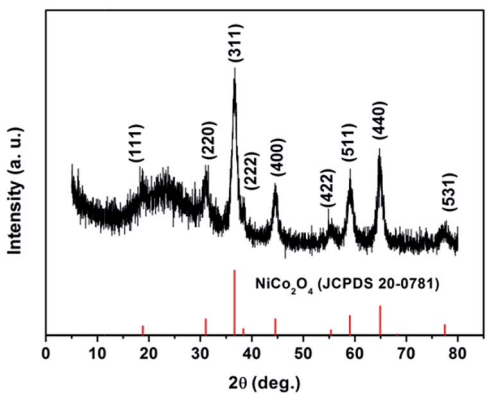

Fig. 2 XRD pattern of the nanorod-assembled $NiCo_2O_4$ hollow microspheres.

As shown in Fig. 4, the possible formation mechanism of a $NiCo_2O_4$ hollow microsphere is proposed. The formation of the $NiCo_2O_4$ hollow structure is mainly caused by the ionic liquid [Bmim]Cl. The ionic liquid [Bmim]Cl has dual roles and acts not only as a solvent but also as a template during the synthesis process, and it is vital for the structure of the $NiCo_2O_4$ hollow microspheres. It is well known that ionic liquids could show aggregation behavior and form micelles in solution.[35,36] When [Bmim]Cl was added into the Ni^{2+} and Co^{2+} ion-containing water solution, [Bmim]Cl is soluble in water to a certain extent with stirring, and it can be dispersed into small droplets to form numerous micelles, where the hydrophilic group faces outward and the hydrophobic alkyl chain faces inward, forming a two-phase interface. After further adding urea into the above mixed solution, cobalt–nickel bimetallic carbonate hydroxide crystal nuclei were formed through the reaction of the metal cations (Co^{2+} and Ni^{2+}) with the CO_3^{2-} and OH^- anions slowly released from the hydrolysis of urea.[34] Due to the low surface energy of ionic liquid [Bmim]Cl, a large number of cobalt–nickel bimetallic carbonate hydroxide crystal nuclei were easily adsorbed on the surface of the ionic liquid micelles. Under the hydrothermal reaction conditions, these crystal nuclei further grow and self-assemble into nanorods, and finally the precursor of the $NiCo_2O_4$ hollow structure can be formed after washing away the ionic liquids. After calcination, $NiCo_2O_4$ hollow microspheres can be obtained. According to the previously reported literature,[37] only urchin-like $NiCo_2O_4$ solid microspheres can be obtained *via* the hydrothermal synthesis route using urea as precipitant without adding ionic liquid. Therefore, the ionic liquid [Bmim]Cl plays a vital role in the formation of the $NiCo_2O_4$ hollow structure in the synthesis process. The formation process is similar to that in previous reports of BiOI hollow microspheres[38] and graphite-like C_3N_4 hybridized a-Fe_2O_3 hollow microspheres.[29] However, further research is still needed to investigate the exact formation mechanism, which will form part of our future work.

In order to demonstrate the advantages of this unique hollow structure, cyclic voltammetry, galvanostatic charge–discharge measurements and cycling stability tests were used to evaluate the electrochemical properties of the nanorod-assembled $NiCo_2O_4$ hollow microspheres, as displayed in Fig. 5. Fig. 5a shows the CV curves of the $NiCo_2O_4$ hollow microsphere electrode at scan rates of 2–100 mV s^{-1} in a potential range of 0–0.55 V in 2 M KOH solution. A couple of redox peaks can be clearly observed from all the CV curves, which indicates the pseudocapacitive characteristics derived from the faradaic redox reaction related to M–O/M–O–OH, where M represents the Ni and Co ions.[7,10] Moreover, it can be seen from Fig. 5a that the peak currents increase with the increasing scan rates from 2 to 100 mV s^{-1}. Even at a high scan rate of 100 mV s^{-1}, the CV curve doesn't show any obvious distortion, and the position of the anodic or cathodic peak only shifts slightly, suggesting the good electrochemical reversibility and fast charge–discharge characteristics of the $NiCo_2O_4$ hollow microsphere electrode. Fig. 5b displays the galvanostatic charge–discharge curves of the $NiCo_2O_4$ hollow microsphere electrode at current densities of 2–30 A g^{-1} in a potential range

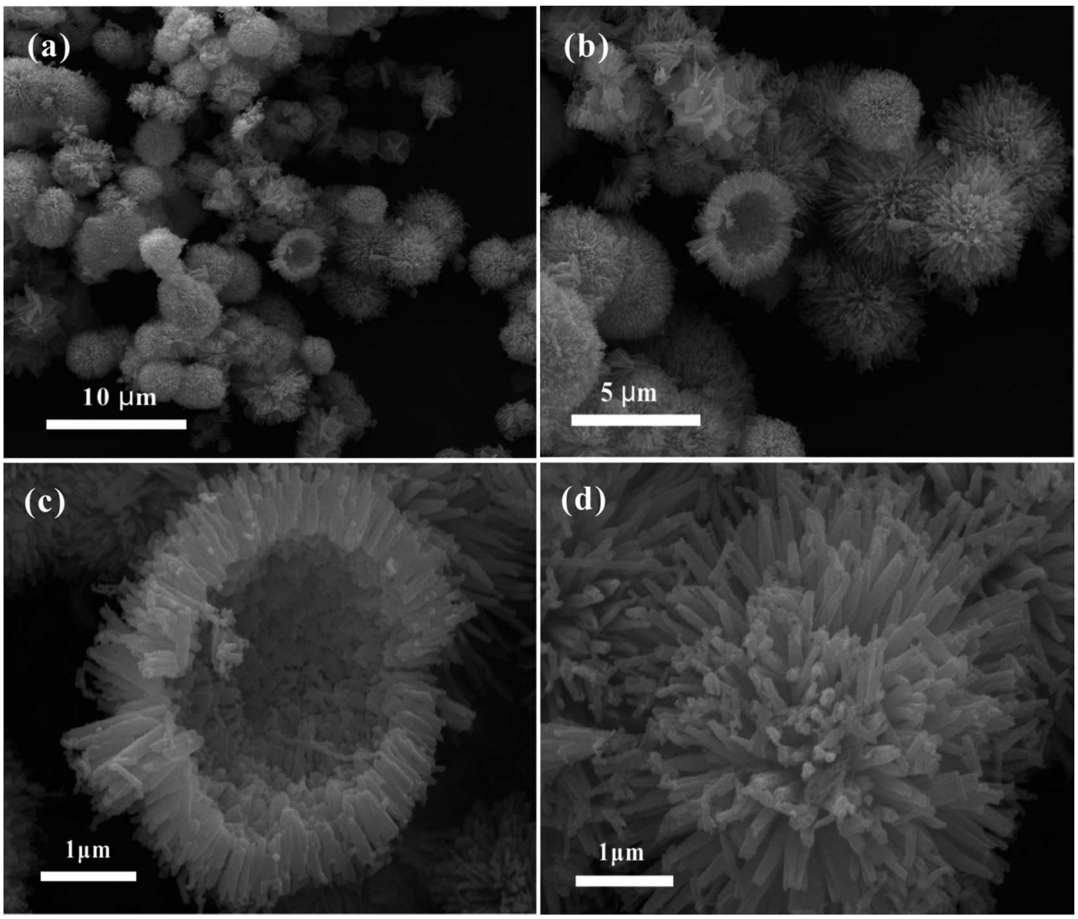

Fig. 3 SEM images of the nanorod-assembled $NiCo_2O_4$ hollow microspheres under different magnifications.

of 0–0.5 V in 2 M KOH solution. The calculated specific capacitance of the $NiCo_2O_4$ hollow microsphere electrode as a function of current density is plotted in Fig. 5c. The specific capacitances of the $NiCo_2O_4$ hollow microsphere electrode are calculated to be 764, 717, 620, 517 and 449 F g^{-1} at current densities of 2, 5, 10, 20 and 30 A g^{-1}, and the capacity retention rate (compared with 2 A g^{-1}) is as high as 53.5% at a current density of 30 A g^{-1}, indicating the superior rate capability. As shown in Fig. 5d, the cycling stability of the $NiCo_2O_4$ hollow microsphere electrode was further estimated by the repeated

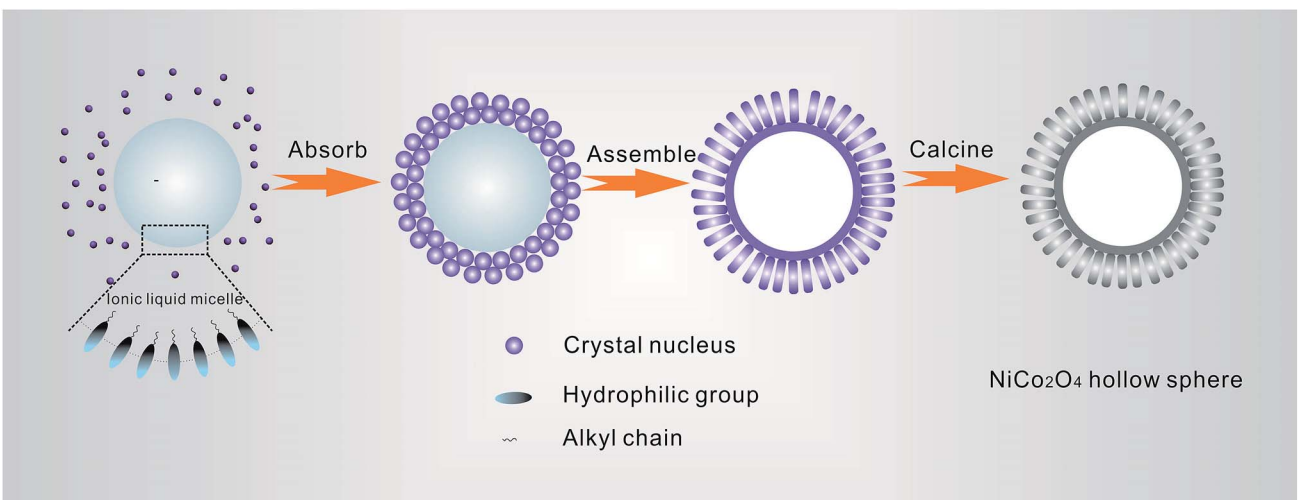

Fig. 4 Formation mechanism of the nanorod-assembled $NiCo_2O_4$ hollow microspheres.

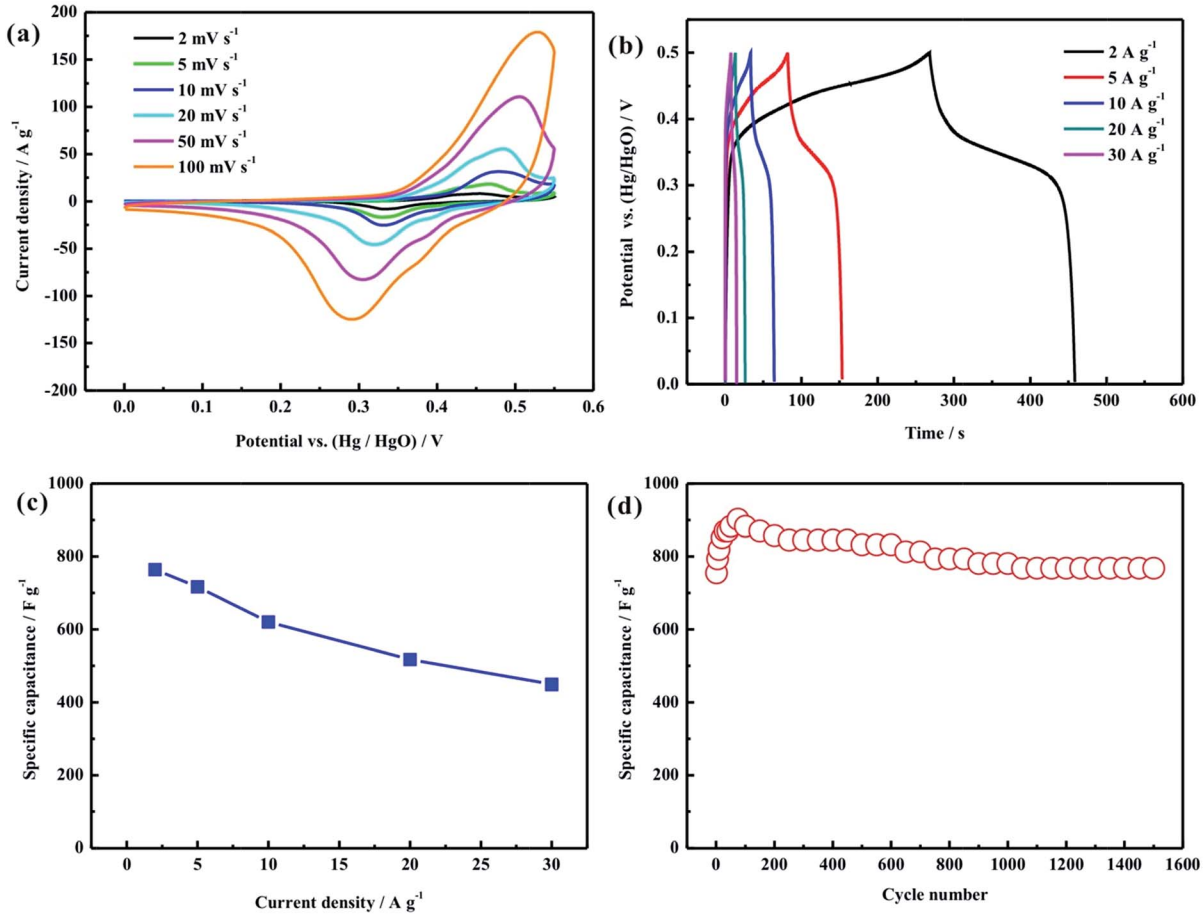

Fig. 5 The nanorod-assembled $NiCo_2O_4$ hollow microsphere electrode: (a) CV curves at scan rates of 2–100 mV s^{-1}; (b) galvanostatic charge–discharge curves at current densities of 2–30 A g^{-1}; (c) the specific capacitance change as a function of current density; (d) the cycling stability at a current density of 2 A g^{-1} for 1500 cycles.

charge–discharge measurement at a current density of 2 A g^{-1}. The specific capacitance of the $NiCo_2O_4$ hollow microsphere electrode increases in the first 80 cycles, which can be ascribed to the cycling-induced improvement of the surface wetting of the electrode, resulting in more electroactive surface areas, and then gradually decreases with cycling numbers and remains stable at about 1000 cycles. This phenomenon is similar to that in many other groups' reports.[12,15,16,18,20] After 1500 cycles, the electrode can retain 101.7% of its initial specific capacitance.

The superior electrochemical performance of the $NiCo_2O_4$ electrode can be attributed to the unique nanorod-assembled hollow structure: (1) the tiny nanorod-assembled shell can enlarge the contact area between the electrode and electrolyte, and thus offer more active sites for the faradic redox reaction, resulting in the enhancement of the specific capacitance; (2) the abundant open space between the neighboring nanorods can provide an easy electrolyte penetration path, ensuring the high electrochemical utilization of the active material and an improvement of the high rate capability; (3) the micrometer-sized structure of the hollow sphere can keep the host structure and buffer against volume changes during the charge–discharge process to guarantee good stability.

4. Conclusions

In summary, nanorod-assembled $NiCo_2O_4$ hollow microspheres have been fabricated by a facile ionic liquid-assisted hydrothermal synthesis route for the first time. Due to the advantages of the unique hollow micro-/nanostructure, the as-resulted $NiCo_2O_4$ hollow microspheres demonstrate a high specific capacitance of 764 F g^{-1} at 2 A g^{-1}, remarkable capacity retention rate of 53.5% at 30 A g^{-1} compared with 2 A g^{-1} and superior cycling stability of 101.7% of initial capacity retention over 1500 cycles at 2 A g^{-1}. The superior electrochemical properties will render the nanorod-assembled $NiCo_2O_4$ hollow microspheres as attractive electrode materials for promising applications in supercapacitors. Furthermore, the liquid-assisted synthesis method can be extended to the preparation of other hollow micro-/nanostructured electrode materials for supercapacitors and other energy storage systems.

Acknowledgements

The work is financially supported by the National Natural Science Foundation of China (21601057, 51574120 and

51274093). Project funded by the China Postdoctoral Science Foundation (2016M602425), Scientific Research Fund of the Hunan Provincial Education Department (16C0462), Program for the New Century Excellent Talents in University (NCET-11-0513), and Distinguished Young Scientists of Hunan Province (13JJ1004).

Notes and references

1 P. Simon and Y. Gogotsi, *Nat. Mater.*, 2008, **7**, 845–854.
2 D. Yu, K. Goh, H. Wang, L. Wei, W. Jiang, Q. Zhang, L. Dai and Y. Chen, *Nat. Nanotechnol.*, 2014, **9**, 555–562.
3 Q. Wang, J. Yan and Z. Fan, *Energy Environ. Sci.*, 2016, **9**, 729–762.
4 L. L. Zhang and X. Zhao, *Chem. Soc. Rev.*, 2009, **38**, 2520–2531.
5 Y. Zhu, X. Ji, C. Pan, Q. Sun, W. Song, L. Fang, Q. Chen and C. E. Banks, *Energy Environ. Sci.*, 2013, **6**, 3665–3675.
6 D. P. Dubal, P. Gomez-Romero, B. R. Sankapald and R. Holze, *Nano Energy*, 2015, **11**, 377–399.
7 Z. Wu, Y. Zhu and X. Ji, *J. Mater. Chem. A*, 2014, **2**, 14759–14772.
8 L. Shen, Q. Che, H. Li and X. Zhang, *Adv. Funct. Mater.*, 2014, **24**, 2630–2637.
9 H. Jiang, J. Ma and C. Li, *Chem. Commun.*, 2012, **48**, 4465–4467.
10 G. Q. Zhang, H. B. Wu, H. E. Hoster, M. B. Chan-Park and X. W. Lou, *Energy Environ. Sci.*, 2012, **5**, 9453–9456.
11 G. Zhang and X. W. Lou, *Sci. Rep.*, 2013, **3**, 1470.
12 L. Li, S. Peng, Y. Cheah, P. Teh, J. Wang, G. Wee, Y. Ko, C. Wong and M. Srinivasan, *Chem.–Eur. J.*, 2013, **19**, 5892–5898.
13 G. Zhang and X. W. Lou, *Adv. Mater.*, 2013, **25**, 976–979.
14 Q. Wang, X. Wang, J. Xu, X. Ouyang, X. Hou, D. Chen, R. Wang and G. Shen, *Nano Energy*, 2014, **8**, 44–51.
15 C. An, Y. Wang, Y. Huang, Y. Xu, C. Xu, L. Jiao and H. Yuan, *CrystEngComm*, 2014, **16**, 385–392.
16 Y. Zhu, Z. Wu, M. Jing, W. Song, H. Hou, X. Yang, Q. Chen and X. Ji, *Electrochim. Acta*, 2014, **149**, 144–151.
17 Q. Wang, B. Liu, X. Wang, S. Ran, L. Wang, D. Chen and G. Shen, *J. Mater. Chem.*, 2012, **22**, 21647–21653.
18 C. Yuan, J. Li, L. Hou, J. Lin, G. Pang, L. Zhang, L. Lian and X. Zhang, *RSC Adv.*, 2013, **3**, 18573–18578.
19 L. Shen, L. Yu, X.-Y. Yu, X. Zhang and X. W. Lou, *Angew. Chem., Int. Ed.*, 2015, **54**, 1868–1872.
20 Y. Zhu, Z. Wu, M. Jing, X. Jia and X. Ji, *Electrochim. Acta*, 2015, **178**, 153–162.
21 Y. Zhao and L. Jiang, *Adv. Mater.*, 2009, **21**, 3621–3638.
22 M. Chen, C. Ye, S. Zhou and L. Wu, *Adv. Mater.*, 2013, **25**, 5343–5351.
23 M. Antonietti, D. Kuang, B. Smarsly and Y. Zhou, *Angew. Chem., Int. Ed.*, 2004, **43**, 4988–4992.
24 W. Liu, L. Xu, D. Jiang, J. Qian, Q. Liu, X. Yang and K. Wang, *CrystEngComm*, 2014, **16**, 2395–2403.
25 J. Lian, X. Duan, J. Ma, P. Peng, T. Kim and W. Zheng, *ACS Nano*, 2009, **3**, 3749–3761.
26 J. Zhang, J. Wang, S. Zhou, K. Duan, B. Feng, J. Weng, H. Tang and P. Wu, *J. Mater. Chem.*, 2010, **20**, 9798–9804.
27 X. Liu, X. Duan, Q. Qin, Q. Wang and W. Zheng, *CrystEngComm*, 2013, **15**, 3284–3287.
28 X. Liu, Y. Li, Z. Zheng and F. Zhou, *RSC Adv.*, 2013, **3**, 341–344.
29 L. Xu, J. Xia, H. Xu, S. Yin, K. Wang, L. Huang, L. Wang and H. Li, *J. Power Sources*, 2014, **245**, 866–874.
30 Y. Zhu, X. Ji, Z. Wu, W. Song, H. Hou, Z. Wu, X. He, Q. Chen and C. E. Banks, *J. Power Sources*, 2014, **267**, 888–900.
31 Y. Zhu, Z. Wu, M. Jing, X. Yang, W. Song and X. Ji, *J. Power Sources*, 2015, **273**, 584–590.
32 L. F. Hu, L. M. Wu, M. Y. Liao, X. H. Hu and X. S. Fang, *Adv. Funct. Mater.*, 2012, **22**, 998–1004.
33 A. Trunov, *Electrochim. Acta*, 2013, **105**, 506–513.
34 X. Li, L. Jiang, C. Zhou, J. Liu and H. Zeng, *NPG Asia Mater.*, 2015, **7**, 165–172.
35 J. Yuan, X. Bai, M. Zhao and L. Zheng, *Langmuir*, 2010, **26**, 11726–11731.
36 J. Bowers, C. P. Butts, P. J. Martin and M. C. Vergara-Gutierrez, *Langmuir*, 2004, **20**, 2191–2198.
37 J. Xiao and S. Yang, *RSC Adv.*, 2011, **1**, 588–595.
38 J. Xia, S. Yin, H. Li, H. Xu, Y. Yan and Q. Zhang, *Langmuir*, 2011, **27**, 1200–1206.

